

A Study on the Copper Recovery from the Slag of the Outokumpu Direct-to-Copper Process

MARIAN KUCHARSKI, TOMASZ SAK, PIOTR MADEJ, MACIEJ WĘDRYCHOWICZ, and WIESŁAW MRÓZ

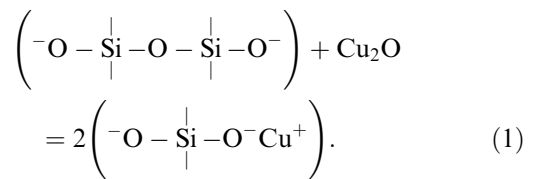
The work was aimed at the investigation of the influence of the carbon reducer's surface on the rate of copper removal from the slag obtained from the flash direct-to-blister process at the Głogów smelter in Poland. It was found that, under our experimental conditions, the copper recovery from the slag slightly increases as the slag/carbon interface increases. It is very likely that the results depend on the geometry of the investigated system as well as the slag foaming phenomenon. The increase of the slag/carbon interface does not noticeably change the final copper content in the slag. The obtained results do not follow any of the reaction rate equations. Therefore, it can be suggested that the slag foaming plays the key role in the experiments by increasing the reduction surface. In addition, the investigated slag has a high viscosity, which hampers the mass transfer in this slag. This hypothesis is supported by the fact that the slag layer situated below the graphite penetrator was found to be of a different color than the slag in the vicinity of that penetrator, where it was agitated by the CO and CO₂ gases generated by the reactions of the slag reduction. Also, the slag in the layer under the penetrator contained more copper than the slag above this layer.

DOI: 10.1007/s11663-013-9961-2

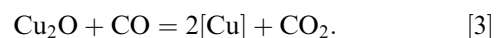
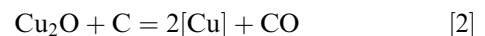
© The Minerals, Metals & Materials Society and ASM International 2013

I. INTRODUCTION

THE Outokumpu direct-to-blister process was commercially implemented for the first time in 1978, in Głogów, Poland. The process requires a high oxygen potential, and therefore it is restricted to those smelting concentrates which mainly consist of minerals without iron (*e.g.*, Cu₂S, CuS, Cu₉S₅) or with a small iron content (Cu₅FeS₄). As a consequence of the high oxygen potential in the Outokumpu flash smelting furnace, the produced slag contains 12 to 16 pct Cu in the Głogów smelter. The copper in the slag constitutes 1/3 of the copper content in the smelting concentrate. Therefore, the recovery of the copper from this slag has a practical importance and heavily influences the operational costs. A part of the copper in the slag is in form of fine inclusions suspended in the slag; however, the majority of the copper is dissolved in it. The slag cleaning process is carried out in an electric furnace with coke and limestone additions. The limestone modifies the reduced slag in order to facilitate the process. Slags are ionic liquids,^[1-3] and the copper in the slags exists mainly as Cu₂O and Cu⁺, associated with the silicate anions, according to the reaction:



Cu₂O is a basic oxide and the oxygen ion in it breaks the bridge in the Si-O network structure, which leads to the dissociation of the silicate anion complexes. During the reduction process, the situation becomes reverse, and the silicate anions undergo polymerization. This model^[4] suggests that the dissolved copper is almost entirely in the form of (-Si-O-Cu⁺), for the slags containing about 1 wt. pct of copper. As such a slag contains a small amount of Cu₂O, it causes sluggishness of the copper recovery process when it is close to completion, because the copper reduction by carbon can proceed only according to the following reactions:



The addition of basic metal oxides (CaO, FeO, ...) to the slag causes some of the copper ionic Cu⁺ to be replaced by Ca²⁺, Fe²⁺, ..., and therefore, the concentration of Cu₂O increases. There are a number of papers^[5-26] devoted to the study on the kinetics of the reduction of FeO and Fe₂O₃ oxides from slags, but only few deal with the reduction of non-ferrous metals from slags. Therefore, an extensive study on the kinetics of copper recovery from industrial slags was undertaken to

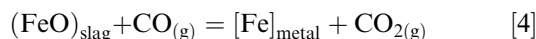
MARIAN KUCHARSKI, Professor, TOMASZ SAK, PIOTR MADEJ, and MACIEJ WĘDRYCHOWICZ, Ph.D. Students, are with the Department of Metallurgy of Non-Ferrous Metals, AGH University of Science and Technology, 30 Mickiewiczza Avenue, 30-059 Kraków, Poland. Contact e-mail: kuch1941@agh.edu.pl WIESŁAW MRÓZ, formerly Researcher with the Department of Metallurgy of Non-Ferrous Metals, AGH University of Science and Technology, is now retired.

Manuscript submitted July 25, 2012.

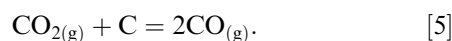
Article published online October 8, 2013.

improve effectiveness of the copper recovery in Głogów smelter. In this study, the influence of the carbon/slag interface on the rate of the copper recovery from the slag of the direct-to-blister flash smelting process was investigated at 1573 K (1300 °C).

Kondakov *et al.*^[5] reported the kinetics measurements of the reduction of molten pure iron oxide by means of solid graphite at the temperature range of 1723 K to 1923 K (1450 °C to 1650 °C). They conducted their experiments in a closed system, measuring the CO gas pressure as a function of time. Knowing the volume of the reaction tube, one can determine the number of the generated CO moles, which should be equivalent to the reduced FeO moles. Under experimental conditions, the mass transport was very fast, and not rate limiting. Therefore, the authors could conclude that the rate-limiting stage was the carbon gasification reaction. Grieveson and Turkdogan^[6] carried out the reduction of pure FeO placed in an iridium crucible at 1823 K (1550 °C). The crucible was placed in a hot zone with the temperature gradient of 1 K (1 °C) between the top and the bottom of the crucible. It eliminated the convective flows in the melt. They used a CO-CO₂ mixture as the reducing agent. For the selected CO₂/CO ratio, they held a sample in the furnace for 17 hours, to establish the equilibrium between the melt and the gas phase, and then the CO₂/CO ratio was changed, to oxidize or reduce FeO. After the completion of the oxidation/reduction process, the sample was quenched very fast and analyzed for Fe²⁺ and Fe³⁺ contents. The authors found out that diffusion was rate-controlling step of the reduction/oxidation process. Krainer *et al.*^[7] reduced FeO from the SiO₂-FeO and SiO₂-FeO-CaO slags with the use of graphite and coke crucibles in a thermobalance. They concluded that the reduction process was controlled by the Boudouard reaction. Fun,^[8] on the other hand, concluded that the kinetics of the reduction of FeO from the SiO₂-CaO-FeO slag cannot be explained either by the diffusion or by the carbon gasification limiting stage. He found that the reduction rate is proportional to the FeO concentration to power 1.77, and he interpreted this fact in the way that the reduction process can be described by convective mechanisms. Shalimov *et al.*^[9] reduced the SiO₂-FeO slag with a graphite sphere at the temperature range of 1573 K to 1723 K (1300 °C to 1450 °C). They found that the activation energy for the reduction was 190 kJ/mol and that the process is controlled by the chemical reaction. According to these authors, the reduction process proceeds in two consecutive stages in the gas phase. The graphite/slag reaction produces the initial amount of CO molecules, which form a small bubble. The CO gas reacts at the slag/gas interface with the slag:



and then, at the gas/graphite interface, CO is reproduced by the Boudouard's reaction:

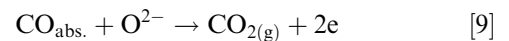
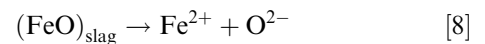


The bubble grows as the reactions proceed, and when it reaches a certain size, the majority of it floats away from the graphite surface. The gas adherent to the graphite surface forms another bubble, which begins to grow according to the above scheme. Sato *et al.*^[12] reduced the pure liquid FeO with solid graphite and with carbon dissolved in liquid iron. The reduction rates were determined from the amount of CO generated during the reduction processes. These authors found that the reduction rate in the case of solid carbon is much lower than in the case when the carbon dissolved in the molten iron reduces the iron oxide. They concluded that the activation energy for the reduction with solid carbon was 313 kJ/mol, while in the case of the carbon dissolved in the molten iron as the reducing agent, the activation energy was 183 kJ/mol.

Utigard *et al.*^[15] studied the copper recovery from the industrial slag (El Teniente converter slag) by using two different CO containing gases. They found that the reduction is controlled by the CO pressure according to the relation:

$$\text{Rate} \left(\frac{\text{mol O}}{\text{m}^2 \text{s}} \right) = 7.9 \times 10^5 \exp \left(\frac{-43,300}{T(\text{K})} \right) \cdot P_{\text{CO}}(\text{Pa}). \quad [6]$$

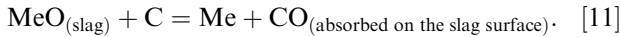
They suggested that the reduction follows the Min and Fruehan's model^[14] for the gas/slag reaction:



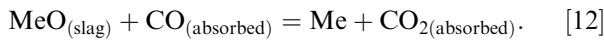
Warczok and Utigard^[18] reduced the synthetic fayalite slags in the temperature range of 1523 K to 1723 K (1250 °C to 1450 °C) using either a floating graphite disk or an immersed graphite rod. They found that the reduction rate per unit area of graphite is significantly higher for the immersed rod than for the floating graphite disk. They concluded that the reduction process is controlled by the Boudouard reaction. El-Rassi and Utigard^[20] investigated the reduction kinetics of the nickel smelting and converting slags under the conditions when alternating or direct current was passing through these slags. They observed that the reduction rate increases with the increasing electric power input and the slag temperature. They also found that the converter slag reduction was almost three times faster than the reduction of the smelting slag. That is because the oxygen potential of the converting slags is approximately 10⁴ to 10⁵ times higher than that of the smelting slags. The authors suggested that the reduction process is controlled by the Boudouard reaction. Mróz^[23] used a

rotating graphite disk for his study on the reduction of FeO from the SiO₂-CaO-FeO liquid slags in the temperature range of 1623 K to 1693 K (1350 °C to 1420 °C). He claimed that the reduction process proceeds under the diffusion control. Barati and Coley^[26] studied the kinetics of the CO-CO₂ reaction with the CaO-SiO₂-FeO-Fe₂O₃ slags, with the CaO/SiO₂ ratio varying between 0.3 and 2. They found that the apparent rate constant increases with the iron oxide content, and with the decreasing of the oxygen partial pressure. The rate constant also increases with temperature and follows the Arrhenius relationship.

As can be seen from this literature review, there is a common understanding that the overall process is initiated by the direct contact of the carbon and the slag:



In the next step, the carbon monoxide absorbed on the slag surface reacts with the metal oxide in the slag:



After the desorption of CO₂ from the slag surface, it diffuses toward the gas-carbon interface and then absorbs on the carbon surface, where the reaction proceeds:



The desorbed CO diffuses toward the gas/slag interface, closing the loop. The overall process can be controlled by:

- (1) the carbon gasification reaction;
- (2) the reduction reaction;
- (3) the metal cation and the associated oxygen anion transport from the bulk of the slag into the slag/gas interface.

It seems that the metal oxide reduction control depends on the parameters accompanying the copper recovery process.

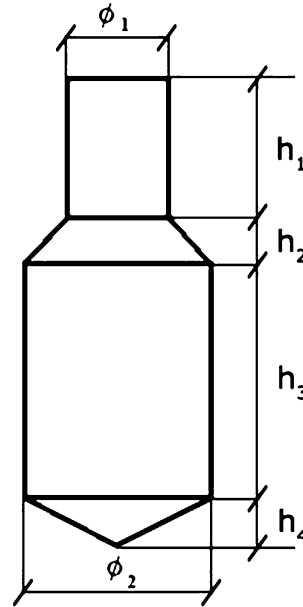


Fig. 2—Shape of the graphite penetrators used in this study.

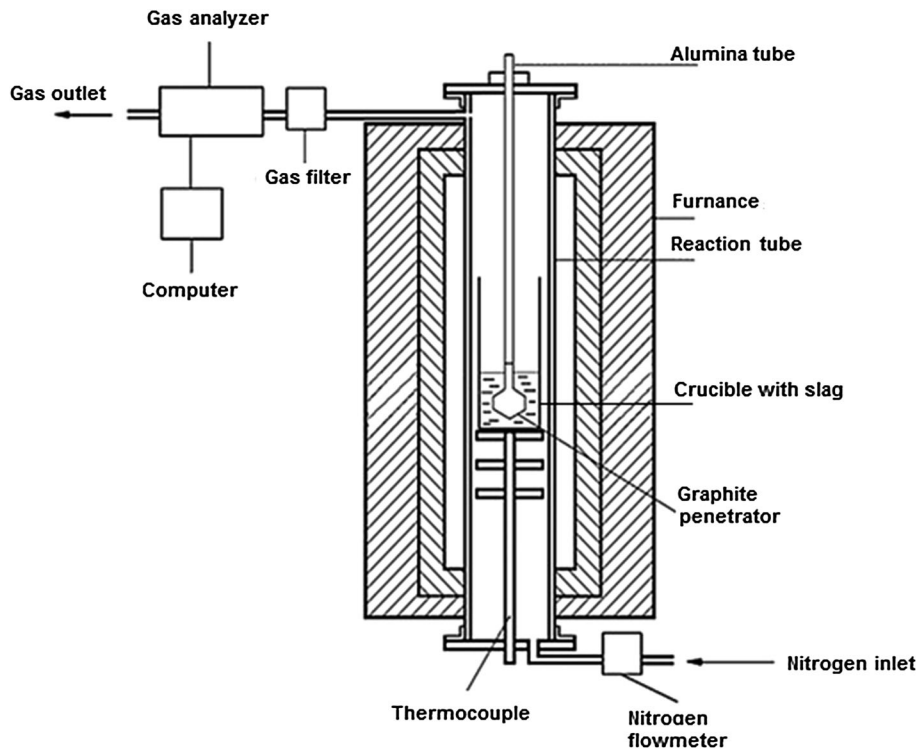


Fig. 1—Experimental apparatus.

II. APPARATUS

A schematic diagram of the apparatus used in this study is shown in Figure 1. It consists of a furnace with Superkantal heating elements, powered by means of a transformer controlled by a Eurotherm controller, which is also connected to a controlling thermocouple Pt-PtRh10. The furnace temperature was maintained at ± 2 K (± 2 °C) and the maximum temperature variation in the hot zone was ± 3 K (± 3 °C). An alumina reaction tube was sealed at the top and the bottom by means of water-cooled brass caps and with the use of rubber O-rings. The measuring thermocouple Pt-PtRh10 was situated close to the crucible with the investigated slag, and it measured the temperature of the sample with a Keithley's multimeter 2000. The graphite penetrators were placed under the upper cap of the reaction tube. The experiment started when the graphite penetrator was transferred into the slag, followed by the temperature stabilization of the molten slag. In this study, the penetrators of different surfaces were used, as can be seen in Figure 2.

The shape of the penetrators was selected in such a manner that the reduction products did not block the reaction surface. Mróz^[23] studied the reduction of the iron oxide from the SiO₂-CaO-FeO slag with a graphite rotating disk. He observed significant fluctuations in the reduction rate, as the reaction gas products blocked the flat disk's surface until the bubble of the CO-CO₂ gas had exceeded a certain size and then flowed out. The same phenomenon was also observed by Warczok and Utigard,^[18] in the case when a flat graphite disk was used as the slag reducer.

The dimensions of these penetrators and their surfaces are given in Table I.

Purified nitrogen of 25 Ndm³/h flow rate was admitted to the reaction tube just after the sample was put into the reaction tube and during the experimental run. The nitrogen flow rate was controlled with the use of an electronic flowmeter manufactured by Brooks. The gas train was made by means of steel tubing connected by Hoke's fittings and valves. During the experiments, a gas composed of nitrogen, carbon monoxide and carbon dioxide was formed as a result of the reactions between the graphite and the slag. The CO and CO₂ concentrations were determined by a gas analyzer for CO and CO₂ every 5 seconds and the results were recorded by the computer.

III. CALIBRATIONS OF THE GAS ANALYZER AND EXPERIMENTAL SET-UP

An infrared gas analyzer was used in this study to analyze CO and CO₂ in the N₂-CO-CO₂ mixture. To speed up the passage of the off-gas through the reaction tube, a nitrogen carrier gas of 25 Ndm³/h flowrate was admitted into the reaction tube of the furnace. For this reason, the gas analyzer had to be calibrated. The calibration was carried out by allowing a passage of a gas mixture containing nitrogen of 25 Ndm³/h flowrate with the additions of predetermined flowrates of CO,

Table I. Dimensions of the Penetrators and Their Surfaces

	Penetrator 1	Penetrator 2	Penetrator 3	Penetrator 4
ϕ_1 (mm)	11	11	11	11
ϕ_2 (mm)	15	20	25	30
h_1 (mm)	15	15	15	15
h_2 (mm)	5	5	5	5
h_3 (mm)	25	25	25	25
h_4 (mm)	5	5	5	5
S (cm ²)	16.1	22.5	29.8	37.9

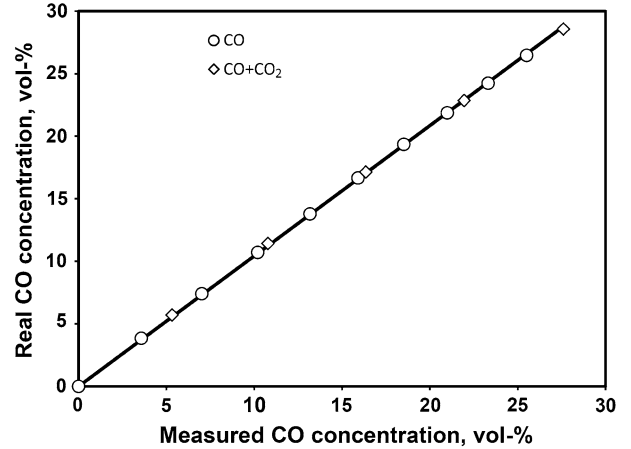


Fig. 3—Correlation between the readings of the gas analyzer for CO and the real carbon oxide concentration in the gas mixture N₂-CO-CO₂ admitted to the reaction tube of the furnace.

CO₂, or CO-CO₂ mixtures. The flowrates of these gases were controlled by Brooks flowmeters and corrected to 273 K (0 °C). The compositions of the gases leaving the furnace were analyzed for CO and CO₂ with a gas analyzer, and the results were recorded by the computer. If the obtained readings of pctCO and pctCO₂ did not change with time, then these values were taken for the calibration procedure. Figure 3 shows the relation between the gas analyzer reading for the CO concentration and the real concentration of CO in the gas mixtures admitted into the reaction tube.

A similar correlation was obtained for CO₂. It was assumed that these correlations can be described by the following relations:

$$(\text{pctCO})_{\text{real}} = A \cdot (\text{pctCO}) \quad [14]$$

$$(\text{pctCO}_2)_{\text{real}} = B \cdot (\text{pctCO}_2), \quad [15]$$

where A is the slope of the calibration straight line for CO, B is the slope of the calibration straight line for CO₂,

$$(\text{pctCO})_{\text{real}} = \frac{100 \cdot V_{\text{CO}}}{V_{\text{N}_2} + V_{\text{CO}} + V_{\text{CO}_2}}$$

(pctCO), (pctCO₂) are the analyzer readings for CO and CO₂, respectively, V_{CO} , V_{CO_2} are the flowrates of CO and CO₂ in (Ndm³/h).

By means of the least squares method and with the use of the calibration results, the A and B coefficients were determined:

$$(\text{pctCO})_{\text{real}} = 1.058 \cdot (\text{pctCO}) \quad [16]$$

$$(\text{pctCO}_2)_{\text{real}} = 0.978 \cdot (\text{pctCO}_2). \quad [17]$$

Relations [16] and [17] were used to develop the formulas for the determination of the flowrates of CO and CO₂ formed during the reduction process:

$$V_{\text{CO}} = \frac{25 \cdot (\text{pctCO})}{94.48 - (\text{pctCO}) - 0.942 \cdot (\text{pctCO}_2)} \quad [18]$$

$$V_{\text{CO}_2} = \frac{25 \cdot (\text{pctCO}_2)}{102.25 - (\text{pctCO}_2) - 1.08 \cdot (\text{pctCO})}. \quad [19]$$

When the penetrator is immersed in the investigated slag, the reduction reactions take place, which generate CO and CO₂. However, the first gas analyzer readings could be detected after about 50 seconds from the moment of the graphite penetrator immersion into the slag. There is no doubt that a part of these gases is cumulated in the reaction tube, and this fraction should be taken into consideration. In order to estimate the real volumes of these gases, the calibration of the reaction tube was carried out. This procedure consists of putting an empty crucible in the reaction tube at 1573 K (1300 °C), while pure nitrogen of 25 Ndm³/h flowrate is passing through the reaction tube. With the tube of the internal diameter of 3 mm situated in the crucible at the level which, during the experiments, was occupied by the slag surface, CO₂ was admitted with the preselected flowrate (1, 2, 3, 4, 5, 6, 7, 8, 9, and 10 Ndm³/h). A change of the CO₂ concentration in the N₂-CO₂ mixture leaving the reaction tube was recorded by the gas

analyzer as a function of time. Figure 4 illustrates the calculated flowrates with Eq. [19] in the case when carbon dioxide of 10 Ndm³/h flowrate was admitted into the reaction tube.

With relation [19] and the simulation results, the volume of CO₂ leaving the reaction tube can be estimated. At the same time, we know the volume of CO₂ admitted into the reaction tube. Therefore, we can estimate the volume of CO₂ cumulated in the reaction tube:

$$\Delta V_{\text{CO}_2} = V_{\text{inlet}} - V_{\text{outlet}}. \quad [20]$$

The values of ΔV_{CO_2} depend on the carbon dioxide flowrate, which is illustrated in Figure 5.

The results were described with the linear equation:

$$\Delta V_{\text{CO}_2}(\text{Ndm}^3) = 0.0219 \cdot V_{\text{CO}_2}(\text{Ndm}^3/\text{h}). \quad [21]$$

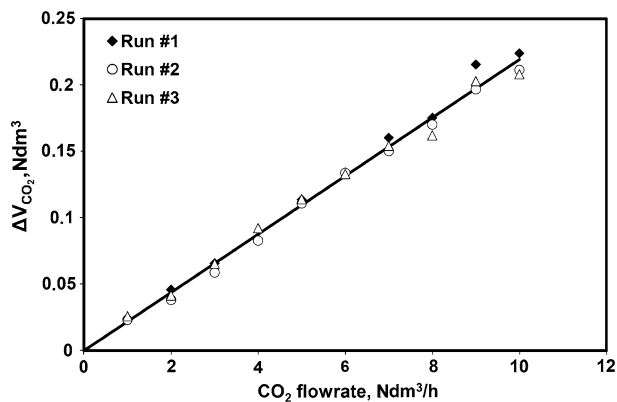


Fig. 5—Dependence of ΔV_{CO_2} vs the carbon dioxide flowrate admitted into the reaction tube at 1573 K (1300 °C).

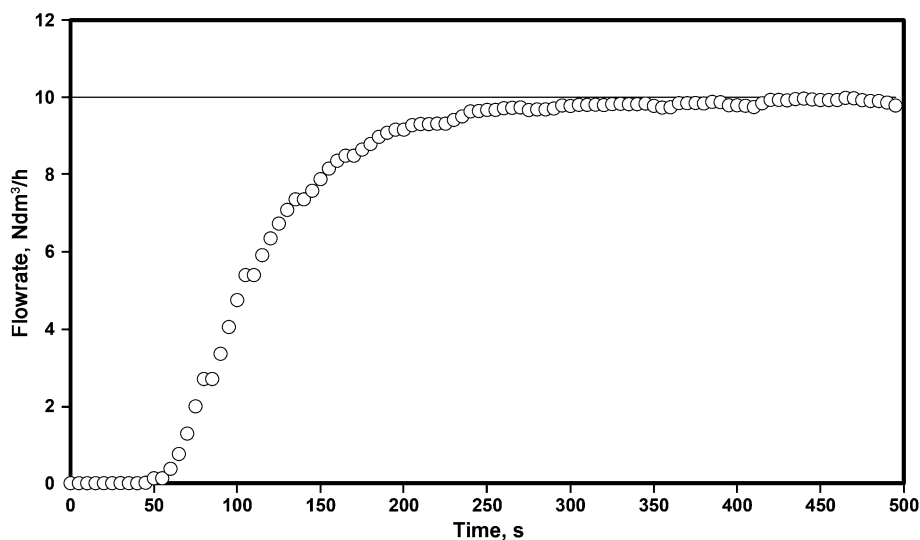


Fig. 4—Calculated flowrates of the CO₂ in N₂-CO₂ mixture leaving the reaction tube vs time, in the case when a stream of CO₂ of 10 Ndm³/h flowrate was used at 1573 K (1300 °C).

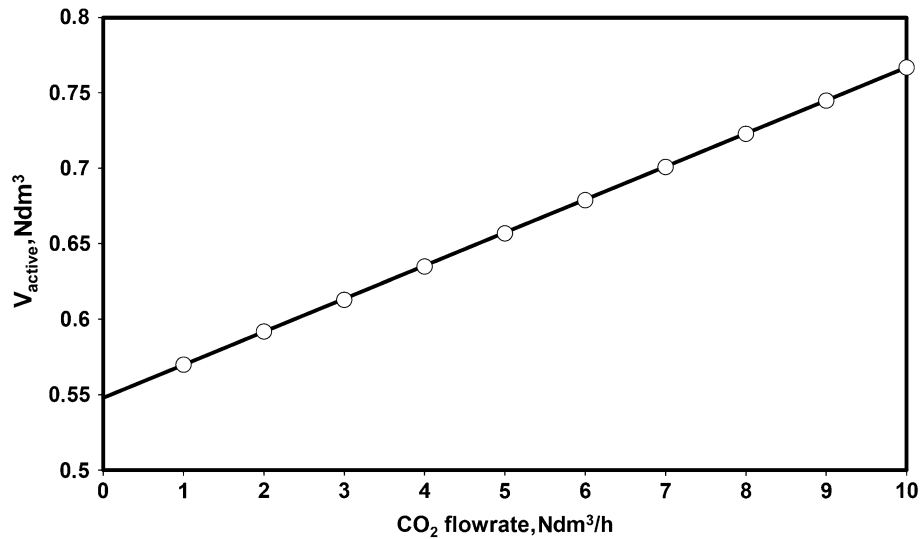


Fig. 6—Dependence of the active volume vs the flowrate of the carbon dioxide admitted into the reaction tube.

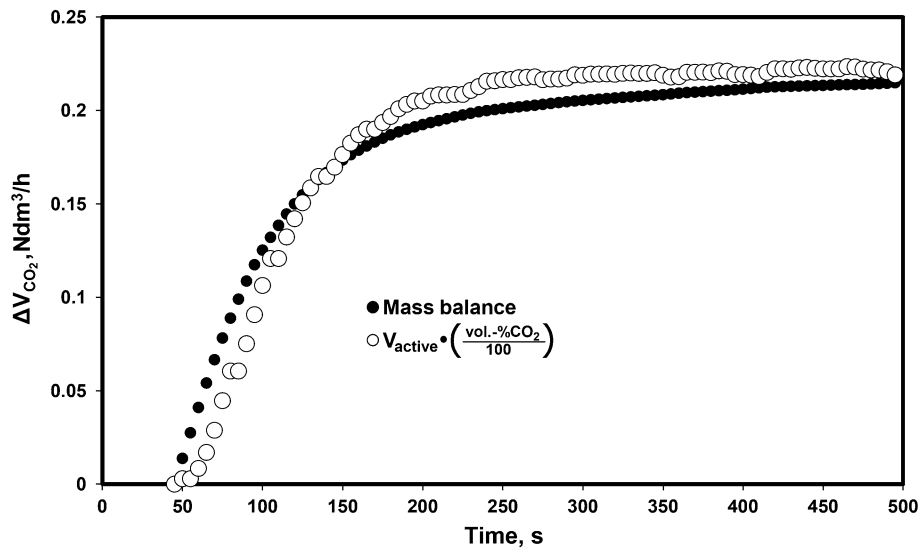


Fig. 7—Comparison of the real ΔV_{CO_2} values (from the mass balance) with the data calculated with Eq. [24]. The simulation was carried out at 1573 K (1300 °C) with a 10 N dm³/h flowrate of CO₂ admitted into the reaction tube.

The total volume of the reaction tube (without a crucible or crucible support) is equal to approximately 3 dm³ and, if we compare it with the values in Figure 5, it becomes clear that the cumulated carbon dioxide occupies only a part of the reaction tube. This part is hereafter called *the active volume*. In every moment, the following relation should be fulfilled:

$$\frac{\Delta V_{\text{CO}_2}}{V_{\text{active}}} = \frac{V_{\text{CO}_2}}{V_{\text{N}_2} + V_{\text{CO}_2}} = \frac{\text{vol.pct CO}_2}{100}, \quad [22]$$

where V_{active} is the active volume of the furnace reaction tube, V_{CO_2} is the flowrate of the carbon dioxide admitted into the reaction tube, V_{N_2} is the flowrate of the nitrogen passing through the reaction tube (equal to 25 Ndm³/h).

With relations [21] and [22], the active volume of the reaction tube was calculated and described with the linear relation:

$$V_{\text{active}}(\text{dm}^3) = 0.548 + 0.0219 \cdot V_{\text{CO}_2}(\text{Ndm}^3/\text{h}). \quad [23]$$

The active volume as a function of the carbon dioxide flowrate is given in Figure 6.

Assuming that, in every moment, the composition of the gas mixture in the active volume is exactly the same as that of the gas leaving the reaction tube, we can calculate the cumulated volume of CO₂ from the relation:

$$\Delta V_{\text{CO}_2} = \frac{(\text{vol.pct CO}_2)}{100} V_{\text{active}}. \quad [24]$$

On the other hand, we can estimate the real volume of CO₂ cumulated in the reaction tube utilizing the mass balance. Figure 7 shows the comparison between the real values of ΔV_{CO₂} (from the mass balance) and those calculated with Eq. [24].

Therefore, the real flowrate of CO₂ passing through the reaction tube after $t = 5i$ seconds can be calculated from the relation:

$$V_{\text{CO}_2(\text{A})}^i = V_{\text{CO}_2}^i + \frac{(\text{vol.} - \text{pctCO}_2)^i - (\text{vol.} - \text{pctCO}_2)^{i-1}}{100} \cdot V_{\text{active}}, \quad [25]$$

where $V_{\text{CO}_2}^i$ is the flowrate of CO₂ estimated with Eq. [19].

The second term of Eq. [25] has to be multiplied by the 3600/5 term, to reconcile the units with $V_{\text{CO}_2}^i$. Figure 8 illustrates the results of the CO₂ flowrate determination with Eq. [25] for the real flowrate of carbon dioxide equaling 10 Ndm³/h.

Assuming that carbon monoxide behaves similarly do carbon dioxide, the following relations can be written:

$$V_{\text{CO}(\text{A})}^i = V_{\text{CO}}^i + \frac{(\text{vol.pctCO})^i - (\text{vol.pctCO})^{i-1}}{100} \cdot V_{\text{active}}, \quad [26]$$

where V_{CO}^i is the flowrate of CO estimated with Eq. [18].

The second term of Eq. [26] has to be multiplied by the 3600/5 term, to reconcile the units with V_{CO}^i .

As the analyzer readings were adjusted to 273 K (0 °C), the numbers of the CO and CO₂ mol generated in 1 second could be calculated from the relations:

$$n_{\text{CO}}^i = \frac{V_{\text{CO}(\text{A})}^i}{22.4 \cdot 3600} \quad [27]$$

$$n_{\text{CO}_2}^i = \frac{V_{\text{CO}_2(\text{A})}^i}{22.4 \cdot 3600}. \quad [28]$$

The number of the oxygen moles removed from the slag during the period of 5 seconds was determined from the relation:

$$n_{[\text{O}]}^{i-1 \rightarrow i} = 5 \frac{n_{\text{CO}}^{i-1} + n_{\text{CO}}^i}{2} + 5 \frac{n_{\text{CO}_2}^{i-1} + n_{\text{CO}_2}^i}{2}, \quad [29]$$

where $n_{\text{CO}}^i, n_{\text{CO}}^{i-1}$ is the number of the CO moles formed during the reduction process per second, calculated for two consecutive measurements, $n_{\text{CO}_2}^i, n_{\text{CO}_2}^{i-1}$ is the number of the CO₂ mole formed during the reduction process per second, calculated for two consecutive measurements.

The masses of the consumed carbon calculated from the Eqs. [27] and [28] were slightly lower than the masses of the graphite used in the experimental runs. The differences were in the order of 0.4 to 4.0 pct which correspond to values estimated in early paper.^[27]

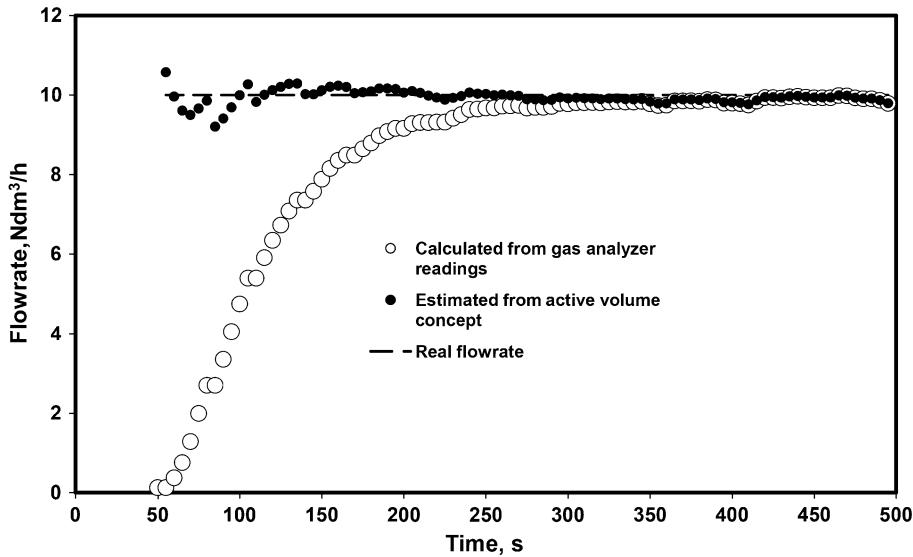


Fig. 8—Estimated real flowrate of carbon dioxide with the active volume concept.

Table II. Main Components of the Głogów Direct-to Blister Flush Smelter Slag used in This Work

Components	Cu	Pb	Fe	Zn	SiO ₂	MgO	CaO	Al ₂ O ₃
Wt. pct	14.31	1.52	7.81	0.87	44.7	3.85	9.0	5.52

IV. EXPERIMENTAL PROCEDURE

A slag produced by the Głogów direct-to-blister flash smelter was used in this study. The main constituents of this slag are listed in Table II.

An alumina crucible (i.d. = 45 mm, H = 77 mm + 200 mm extension) with 160 g of slag was placed in the reaction tube of the furnace. In the upper cap of the

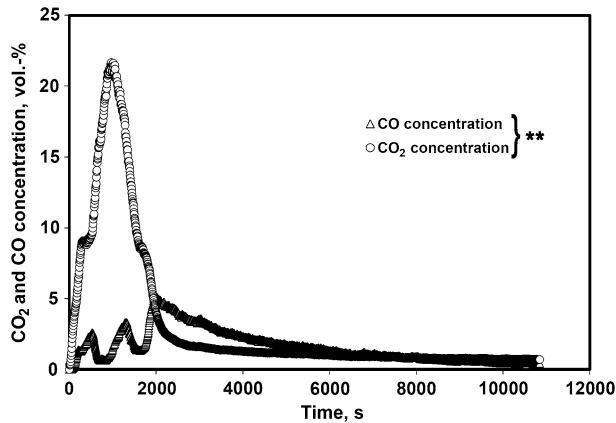


Fig. 9—Gas analyzer readings during the slag reduction. All experimental data in Excel format are available on request.

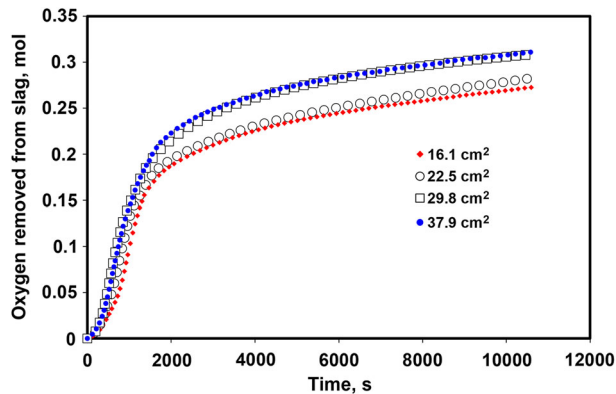


Fig. 10—Relations between the oxygen removed from the slag for penetrators of different surfaces.

reaction tube, a graphite penetrator fixed to an alumina tube was situated. A nitrogen stream of 25 Ndm³/h flow rate was introduced into the reaction tube of the furnace through its bottom cap. After about 5 hours, the furnace was switched on and the temperature controller was adjusted to 573 K (300 °C). The furnace was kept under these conditions for approximately 12 hours. Next, the temperature of the furnace was elevated to 1573 K (1300 °C). The sample was kept at this temperature for 1 hour to attain the temperature stabilization of the molten slag, and then the graphite penetrator was transferred into the slag. The immersion of the graphite penetrator in the slag was taken as the beginning of the reduction process. However, the first signal of the reduction process was detectable after about 50 seconds from that moment. The gas leaving the reaction tube was analyzed for the CO and CO₂ content every 5 seconds by the gas analyzer and the results were recorded by the computer. An example of the obtained results is shown in Figure 9. In the beginning, the temperature of the penetrator was equalizing with the temperature of the slag, and the reduction started to proceed.

The generated CO + CO₂ gas caused the slag foaming process because of the noticeable increase of the CO₂ content observed in the off-gas. For each size of the penetrator, three measurements were conducted. By a summation of the values n_O^i with relation [29], the equation $n_O(t)$ describing the oxygen removed from the slag as a function of the reduction time was determined.

Figure 10 shows an example of these functions obtained for the used penetrators. These curves resemble the plot of the fraction of the sulfur dioxide generated with time by the reaction between the liquid cuprous sulfide and the solid cuprous oxide.^[28]

For every size of the penetrator, three experiments were conducted, and the reduced slags were quenched and analyzed. The obtained results are enclosed in Tables III and IV. The reduced Cu-Pb-Fe alloys were also analyzed and the results are given in Table V. Despite the fact that the samples of these alloys were taken from different places, quite big differences are observed. This is because the Cu-Pb-Fe system exhibits limited solubility in the liquid and the solid state.

Table III. Results of the Chemical Analyses of the Slags Before and After the Reduction Process by Means of Different Graphite Penetrators

Components (wt. pct)	Slag Before Experiments	Penetrator No 1			Penetrator No 2		
		Run 1	Run 2	Run 3	Run 1	Run 2	Run 3
Na ₂ O	0.40	0.66	0.63	0.62	0.67	0.65	0.65
K ₂ O	2.28	3.48	3.43	3.45	3.53	3.61	3.57
CaO	9.00	12.70	12.25	12.34	12.77	12.75	14.26
MgO	3.85	5.13	4.92	4.67	5.05	5.09	5.18
SiO ₂	44.70	47.10	46.90	47.50	48.10	47.00	44.60
Al ₂ O ₃	5.52	13.18	13.91	14.36	13.28	13.94	14.67
Fe	7.81	9.54	9.07	8.58	9.01	9.36	9.80
Zn	0.87	0.94	0.78	0.82	0.84	0.72	0.78
Pb	1.52	1.27	1.05	0.94	0.80	0.76	0.63
Cu	14.31	0.69	1.50	0.58	0.45	0.37	0.38

Table IV. Results of the Chemical Analyses of the Slags Reduced by Means of Different Graphite Penetrators

Components (wt. pct)	Penetrator No 3			Penetrator No 4		
	Run 1	Run 2	Run 3	Run 1	Run 2	Run 3
Na ₂ O	0.64	0.63	0.62	0.64	0.65	0.64
K ₂ O	3.33	3.52	3.46	3.47	3.62	3.52
CaO	12.49	14.12	14.37	14.59	14.40	14.03
MgO	5.03	5.10	4.82	4.97	5.01	5.18
SiO ₂	48.9	46.20	48.30	47.30	48.30	46.80
Al ₂ O ₃	13.36	13.90	14.64	14.36	14.03	13.84
Fe	9.41	9.35	8.89	9.00	8.95	9.23
Zn	0.65	0.76	0.68	0.64	0.63	0.61
Pb	0.69	0.62	0.42	0.33	0.38	0.40
Cu	0.97	0.35	0.34	0.35	0.43	0.28

Table V. Results of the Chemical Analyses of the Cu-Pb-Fe Alloys Obtained During the Slag Reduction by Means of Different Graphite Penetrators

Element (wt. pct)	Penetrator no 1			Penetrator no 2		
	Run 1	Run 2	Run 3	Run 1	Run 2	Run 3
Cu	98.78	96.04	97.89	99.14	99.22	92.75
Fe	0.03	0.01	0.02	0.04	0.01	0.145
Pb	1.31	0.75	1.77	0.49	0.84	7.35

Element (wt. pct)	Penetrator No 3			Penetrator No 4		
	Run 1	Run 2	Run 3	Run 1	Run 2	Run 3
Cu	97.78	94.61	93.17	94.11	94.10	97.73
Fe	0.01	0.00	0.11	0.01	0.00	0.03
Pb	2.08	5.49	6.65	5.26	5.68	1.69

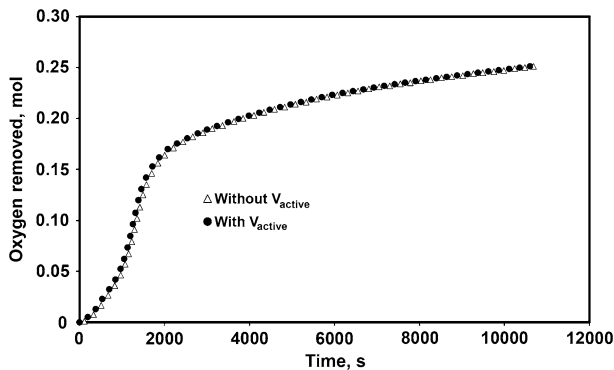


Fig. 11—Comparison of the dependences of the oxygen removed from the slag vs the time estimated with and without the active volume.

V. DISCUSSION

1. In this work, the idea of *active volume* was put forward and estimated for the employed set-up. By way of utilizing this idea, the reaction gases cumulated in the reaction tube can be estimated quantitatively. There was the hope that taking into account the gas cumulated in the reaction tube would make it possible to overcome the difficulties in describing the

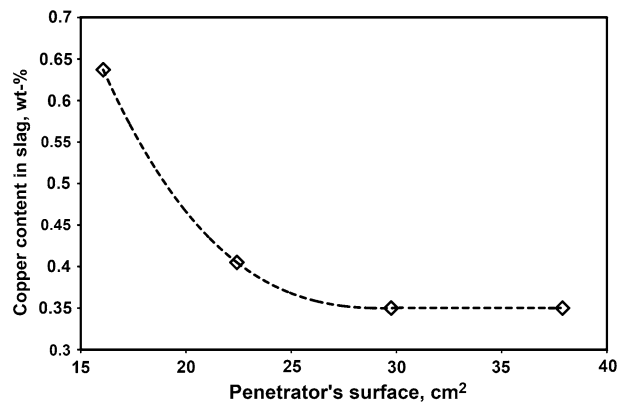


Fig. 12—Relation between the copper final content (mean value from three measurements) and the penetrator's surface.

obtained results with the use of the standard kinetics equations. Unfortunately, this approach did not significantly alter the obtained results, which is demonstrated in Figure 11.

2. The influence of the reducer's surface on the rate of the slag de-coppering process is demonstrated in Figure 12. It is clear that, during the de-coppering process, the copper, lead, and iron are reduced simultaneously but at different rates, forming the

Cu-Pb-Fe alloy. The employed experimental technique is unable to determine the reduction rates of the particular metal oxides.

Figure 12 suggests that the effectiveness of the slag de-coppering process increases with the increase of the penetrator's surface, yet only to some extent. The further increase of the slag/carbon interface does not result in the noticeable lowering of the copper content in the slag after the reduction process. A small influence of the reaction surface on the effectiveness and kinetics of the de-coppering process can be explained by the fact that, at the beginning, the reduction takes place on the slag/penetrator interface, and then, after the bubble detachment—on the gas/slag film of the bubbles. These bubbles form a foam layer, whose stability and bubble size depend on the viscosity, density, and surface tension of the slag.^[29–34] As the interface CO-CO₂ gas/slag film of the bubbles can be much larger than the penetrator's surface, the penetrator surface plays a limited role in the reduction process. In an earlier investigation of the slag from the direct-to-copper process,^[35] X-ray fluorescence images of the slag were taken, showing that the foam height exceeds the height of the reduced slag, as can be seen in Figure 13. The slag foam layer begins from the middle of the graphite penetrator and ends beyond the area of the picture (Figure 13(b)). In the foam image, the dark dots represent the Cu-Pb-Fe droplets which were formed during the reduction of the slag bubble film. However, the estimation of the overall surface of the foam is not possible because the viscosity of the slag increases almost three times between the beginning and the end of the process.^[36] The foaming of the investigated slag was very likely, as the changes of the CO and CO₂ contents in the off-gas vs time in these experiments were very similar to those observed in the earlier investigation.^[35]

In order to explain this phenomenon, let us consider the reduction of copper oxide in a slag by means of a CO₂-CO gas mixture:



Table V shows that the reduced Cu-Pb-Fe alloy contained more than 92 wt. pct Cu, and this fact legitimizes the assumption that the copper activity is close to unity. Utilizing the thermodynamic data^[37] for this reaction, one can estimate the $P_{\text{CO}_2}/P_{\text{CO}}$ ratio in equilibrium of the reaction [30] at 1573 K (1300 °C):

$$\left(\frac{P_{\text{CO}_2}}{P_{\text{CO}}}\right)_{\text{Reduction}} = 1.217 \times 10^3 a_{\text{Cu}_2\text{O}}. \quad [31]$$

The consumed CO is reproduced on the graphite penetrator's surface by the Boudouard's reaction:



At the temperature of 1573 K (1300 °C), the value of the CO₂/CO ratio for the Boudouard's reaction can also be estimated with the use of the thermodynamic data:^[37]

$$\left(\frac{P_{\text{CO}_2}}{P_{\text{CO}}}\right)_{\text{Boudouard}} \approx \frac{1}{2.755 \times 10^3}. \quad [33]$$

Taking into account the relations [31] and [33], one can set up the condition for the copper oxide reduction in the slag:

$$a_{\text{Cu}_2\text{O}} > 2.98 \times 10^{-7}. \quad [34]$$

The limiting value of the activity coefficient of the copper oxide in these slags is larger than unity ($\gamma_{\text{Cu}_2\text{O}}^0 \approx 3.1$).^[4] Assuming that the copper oxide is the only reducible species, the final copper content in these slags should be of the order of 10⁻⁵ wt. pct. In reality, the copper, lead, and iron oxides are reduced simultaneously, and in such a case, the limiting copper content in these slags is of the order of 10⁻² to 10⁻³ wt. pct.^[38,39] In these experiments, the reduction process was proceeding continuously all the time, which is proved by the systematic increase of the number of the oxygen moles removed from the slag (Figure 10). However, after some

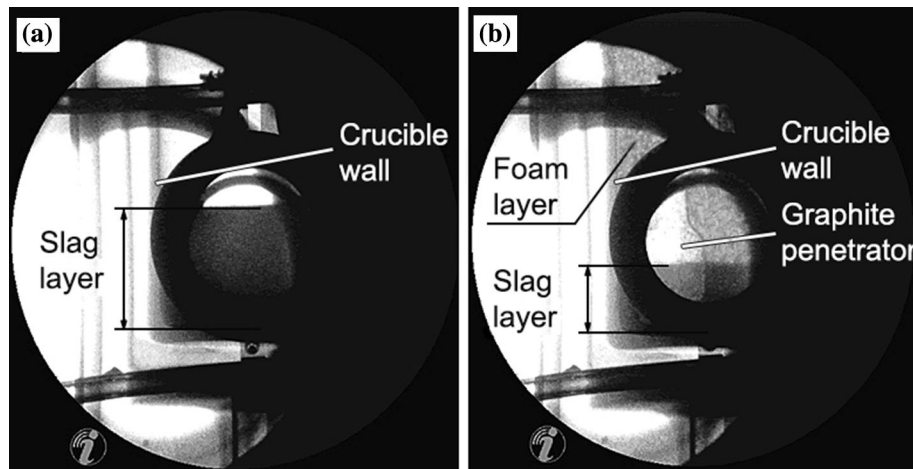


Fig. 13—X-ray fluoroscopic images of the slag with the direct-to-copper process^[35] before (a) and after (b) the immersion of the graphite penetrator.

time, the rate of this reduction became very low. The sluggishness of this process is caused by the lowering of the diffusion rate of Cu_2O in the direction of the slag/ CO_2 - CO gas interface. In addition, when the copper content in the slag decreases considerably, the probability of the CO - CO_2 bubble formation is hampered. For the CO - CO_2 gas bubble to be formed, the following condition should be fulfilled:

$$P_{\text{CO}_2} + P_{\text{CO}} > P_{\text{atm.}} + g\rho_{\text{slag}}h + \frac{2\sigma_{\text{slag}}}{r}, \quad [35]$$

where $P_{\text{atm.}}$ is the atmospheric pressure, g is the gravitational constant, ρ_{slag} is the slag density, h is the depth in which the bubble is formed, σ_{slag} is the slag's surface tension, and r is the radius of the bubble.

Under experimental conditions, the second term of the relation [35] is negligible in comparison with the first and the third one. The atmospheric pressure is constant; however, the third term of the Eq. [35] becomes very large at the moment of the bubble formation. After the copper content in the slag has been considerably lowered, a bubble can be formed only if a sufficient compositional fluctuation in the slag occurs on the slag/graphite interface, which secures the sufficiently high Cu_2O content in a very limited area of this interface. When the Cu_2O concentration decreases continuously, the probability of such fluctuation also decreases. All these phenomena influence the decrease of the reduction rate.

3. The attempts to describe the obtained results with the kinetics equation of the first, second, or n th order failed. However, the rate of the reduction process referred to initial reduction area can be estimated directly with the utilization of the experimental data:

$$\frac{dn_{\text{O}}^i}{dt} \approx \frac{1}{S_{\text{init.}}} \cdot \frac{n_{\text{O}}^i - n_{\text{O}}^{i-1}}{5}, \quad [36]$$

where $n_{\text{O}}^i; n_{\text{O}}^{i-1}$ is the numbers of the oxygen moles removed from the slag after $5i$ and $5(i-1)$ seconds of the reduction time, $i = 1, 2, 3, \dots, k$ is the numbers of the experimental points, $S_{\text{init.}}$ is the penetrator's surface. The estimated values of dn_{O}^i/dt for the used penetrators are illustrated in Figure 14.

It is easy to notice that, in all the cases, the rate of the process increases very rapidly, and after some time, decreases quite fast. The maximum process rate decreases as the initial penetrators surface increase. One would end up with a false conclusion that the rate constant decreases with the increase of the penetrator's surface.

This phenomenon can be explained by way of analyzing the mechanism of the slag foaming for the cases of limiting sizes of the used penetrators. Figure 15 shows a mutual position of the limiting penetrators and the crucible during the experiments. When we used the penetrator with the biggest surface, the gap between the penetrator and the crucible wall is much smaller than in the case when the smallest penetrator is used.

When the penetrator with the biggest size (surface) is used, the most of the generated gases traveling through

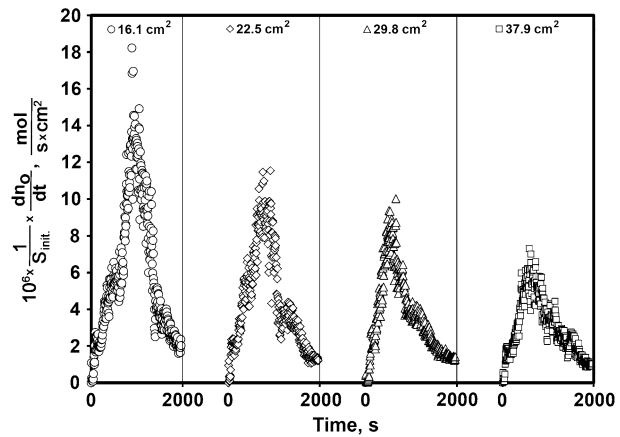


Fig. 14—Rate of the oxygen removal from the investigated slag for penetrators of different surfaces.

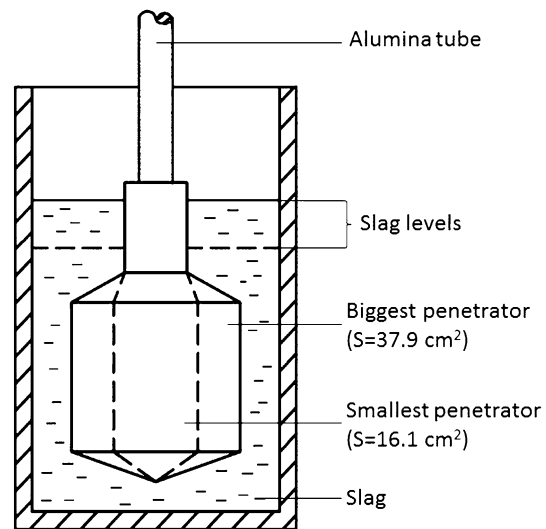


Fig. 15—Schematic representation of a mutual position of the penetrators (the biggest-solid line and the smallest-dashed line) and the crucible wall during experiments.

the cross section area between the penetrator and the crucible wall. This area was almost two times smaller than in the case when the smallest penetrator was used. In consequence, the superficial gas velocities are very different, as can be seen in Figure 16.

According to the literature,^[29,40] the thickness of a foam layer is proportional to the superficial gas velocity. In consequence, for the biggest penetrator in use, the foam layer will be much thicker than for the smallest one. Therefore, with the use of the biggest penetrator, its surface, in a considerable fraction, would be immersed in the foam, and only a smaller portion—in the liquid slag (Figure 13(b)). A part of the CO enclosed in the foam bubbles could be consumed in the reduction process, which increases the efficiency of the carbon utilization. However, at the same time, the active surface of this penetrator decreases very much. In consequence, the maximum of the reduction rate (dn_{O}/dt) referred to

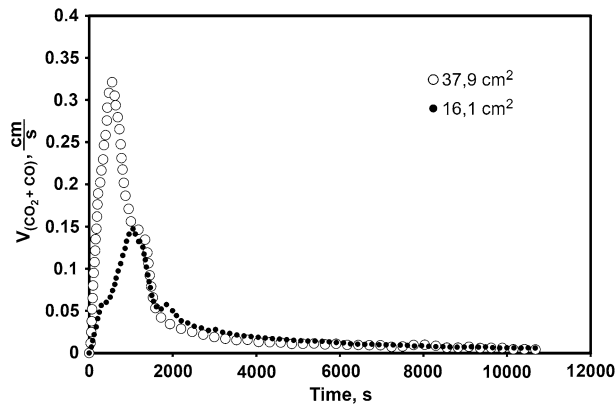


Fig. 16—Relation between the superficial gas velocity and the time for limiting sizes of the graphite penetrators.

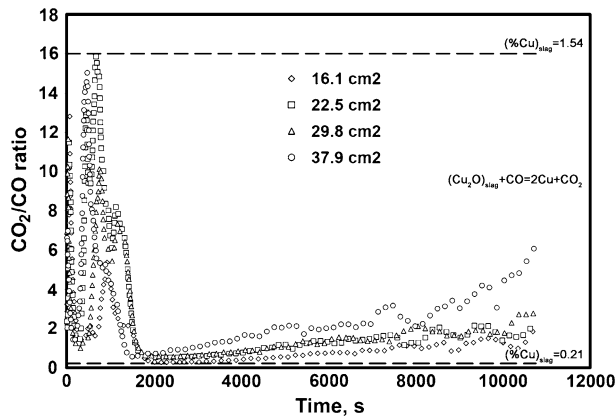


Fig. 17— CO_2/CO ratio vs the time for penetrators of different surfaces.

the penetrator's surface is the smallest for the penetrator with the biggest surface.

In addition, as the gas inside the bubbles which form the foam layer are separated from the graphite penetrator, the Boudouard reaction cannot proceed, and therefore, the off-gas composition should be close to that characteristic for the equilibrium of the reaction Eq. [30]. Figure 17 illustrates the variation of the CO_2/CO ratio vs the time recorded for the penetrators having different surfaces. Figure 17 shows that the CO_2/CO ratio was in the range from approximately 0.2 to 16. For this CO_2/CO ratio, in equilibrium with the slags from the Głogów smelter, the copper content is approximately equal to 0.21 and 1.54 pct, respectively.^[4] It means that the reduction process was controlled by the rate of the reaction Eq. [30]. The investigated slag has a high viscosity, which increases during the reduction process (from 750 to 2200 mPa s at 1573 K (1300 °C)^[36]), and it hampers the mass transfer in this slag. This hypothesis is supported by the fact that the slag layer of about 5 mm in thickness, situated below the penetrator, was of a different color than the slag in the vicinity of that penetrator, where it was agitated by the CO and CO_2 gases, generated by the reduction reactions. This part of the slag apparently contained more copper than the slag above this layer.

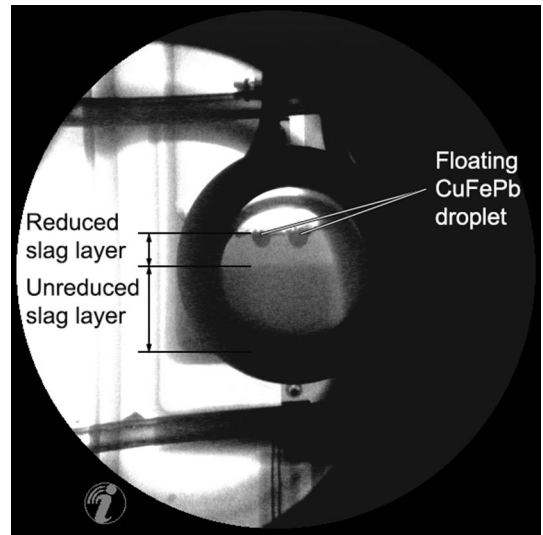


Fig. 18—X-ray fluoroscopic image of the slag from the direct-copper process reduced by grinded graphite applied on its surface at 1573 K (1300 °C).^[35]

This view is also supported by the earlier investigation,^[35] in which grinded graphite was applied on the stagnant slag surface. Figure 18 shows that, after some time, the upper part of the slag became brighter (contained less copper, lead and iron) than that close to the bottom.

It is clear that, in the case of the luck slag agitation, the mass transport is the rate-controlling step of the reduction process. Surprisingly, the reduced Cu-Pb-Fe alloy droplets were floating on the slag surface (Figure 18).

ACKNOWLEDGMENTS

We would like to thank the Polish National Center Research and Development (NCBiR) for the financial support—Grant No. 07-0022-10.

REFERENCES

1. G.W. Toop and C.S. Samis: *Trans. TMS AIME*, 1962, vol. 224, pp. 878–87.
2. C.R. Masson: *Proc. R. Soc. Lond. A*, 1965, vol. A287, pp. 201–221.
3. D.R. Gaskell: *Metall. Trans.*, 1973, vol. 4, pp. 185–92.
4. M. Kucharski: *Met. Technol.*, 1979, vol. 6, pp. 354–56.
5. V.V. Kondakov, D.I. Ryzhonkov, and D.M. Golenko: *Izv. Vuz Chern. Met.*, 1960, vol. 4, pp. 23–28.
6. P. Grieveson and E.T. Turkdogan: *AIME Trans.*, 1964, vol. 230, pp. 1609–614.
7. H. Krainer, H.P. Beer, and H. Brandl: *Techn. Mitt. Krupp. Forsch. Ber.*, 1966, vol. 24 (3), pp. 139–46.
8. F. Fun: *Metall. Trans.*, 1970, vol. 1, pp. 2537–41.
9. M.P. Shalimov, V.N. Boronenkov, and S.A. Lyamkin: *Metally*, 1980, vol. 6, pp. 32–36 (in Russian).
10. Y. Sasaki, S. Hara, D.R. Gaskell, and G.R. Belton: *Metall. Trans. B*, 1984, vol. 15B, pp. 563–71.
11. S.K. El-Rahaiby, Y. Sasaki, D.R. Gaskell, and G.R. Belton: *Metall. Trans. B*, 1986, vol. 17B, pp. 307–316.
12. A. Sato, G. Aragane, K. Kamihira, and S. Yoshimatsu: *Trans. ISIJ*, 1987, vol. 27, pp. 789–96.

13. S. San, Y. Sasaki, and G.R. Belton: *Metall. Trans. B*, 1988, vol. 19B, pp. 959–65.
14. D.J. Min and R.J. Fruehan: *Metall. Trans. B*, 1992, vol. 23B, pp. 29–37.
15. T. Utigard, G. Sanchez, J. Manriquez, A. Lurashi, C. Diaz, D. Cordero, and E. Almendras: *Metall. Mater. Trans. B*, 1997, vol. 28B, pp. 821–26.
16. S. San and G.R. Belton: *Metall. Mater. Trans. B*, 1998, vol. 29B, pp. 137–45.
17. S.R. Story, B. Sarma, R.J. Fruehan, A.W. Cramb, and G.R. Belton: *Metall. Mater. Trans. B*, 1998, vol. 29B, pp. 929–32.
18. A. Warczok and T.A. Utigard: *Can. Metall. Q.*, 1998, vol. 37 (1), pp. 27–38.
19. D.J. Min, J.W. Han, and W.S. Chung: *Metall. Mater. Trans. B*, 1999, vol. 30B, pp. 215–21.
20. K.P. El-Rassi and T.U. Utigard: *Metall. Mater. Trans. B*, 2000, vol. 31B, pp. 1187–94.
21. S.R. Story and R.J. Fruehan: *Metall. Mater. Trans. B*, 2000, vol. 31B, pp. 43–54.
22. S. Sun and S. Jahanshahi: *Metall. Mater. Trans. B*, 2000, vol. 31B, pp. 937–43.
23. J. Mróz: *Metall. Mater. Trans. B*, 2001, vol. 32B, pp. 821–30.
24. Y. Li and I.P. Ratchev: *Metall. Mater. Trans. B*, 2002, vol. 33B, pp. 651–60.
25. M. Barati, E. Chen, and K. Coley: *VII International Conference on Molten Slags, Fluxes and Salts*, The South African Institute of Mining and Metallurgy, 2004, pp. 393–98.
26. M. Barati and K. Coley: *Metall. Mater. Trans. B*, 2005, vol. 36B, pp. 169–78.
27. K. Rogóż and M. Kucharski: *Arch. Metall. Mater.*, 2010, vol. 55, pp. 317–23.
28. D.A. Reeve and T.R. Ingraham: *Can. Metall. Q.*, 1971, vol. 10 (1), pp. 19–20.
29. K. Ito and R.J. Fruehan: *Metall. Trans. B*, 1989, vol. 20B, pp. 509–514.
30. K. Ito and R.J. Fruehan: *Metall. Trans. B*, 1989, vol. 20B, pp. 515–21.
31. Y. Ogawa, D. Huin, H. Gaye, and N. Tokumitsu: *ISIJ Int.*, 1993, vol. 33, pp. 224–32.
32. B. Ozturk and R.J. Fruehan: *Metall. Mater. Trans. B*, 1994, vol. 26B, pp. 1086–88.
33. Y. Zhang and R.J. Fruehan: *Metall. Mater. Trans. B*, 1994, vol. 26B, pp. 1088–91.
34. M. Zhu and D. Sichen: *Steel Res.*, 2000, vol. 71 (3), pp. 76–82.
35. K. Rogóż: Ph.D. Thesis (in Polish), AGH University of Science and Technology, 2009.
36. M. Wędrychowicz and M. Kucharski: unpublished research.
37. A. Roine, J. Mansikka-aho, T. Kotiranta, P. Bjorklund, and P. Lamberg: HSC Chemistry 7.0 software.
38. M. Kucharski: *Arch. Metall. Mater.*, 1981, vol. 26, pp. 3–10.
39. Z. Śmieszek: *Arch. Metall. Mater.*, 1986, vol. 31, pp. 579–661.
40. Y. Zhang and R.J. Fruehan: *Metall. Mater. Trans. B*, 1995, vol. 26B, pp. 803–812.